American Mineralogist, Volume 65, pages 1103–1118, 1980

The gedrite–anthophyllite solvus and the composition limits of orthoamphibole from the Post Pond Volcanics, Vermont

FRANK S. SPEAR

Department of Earth and Planetary Sciences
Massachusetts Institute of Technology
Cambridge, Massachusetts 02139

Abstract

Coexisting orthoamphiboles (high Al–Na gedrites and low Al–Na anthophyllites) from the Post Pond Volcanics, Vermont, display a variety of textures that are interpreted to be equilibrium growth textures. These textures include: (1) discrete grains; (2) bladed intergrowths; (3) patchy intergrowths; (4) overgrowths; and (5) lamellar intergrowths with lamellae parallel to (120). Coexisting orthoamphiboles display exsolution parallel to (010); exsolution is much more pronounced in gedrite than in anthophyllite, which suggests that the solvus is steeper on the anthophyllite limb.

The solvus is defined by discontinuities in the amount of Si, Al^{IV}, Al^{VI}, and Na(A) in the orthoamphiboles, which can be described as gaps in the edenite ($NaAl \rightleftarrows \square Si$) and tschermakite ($Al^{VI}Al^{IV} \rightleftarrows MgSi$) substitutions. The width of the solvus is a function of Fe/(Fe+Mg), with Fe-rich samples showing the widest gap. Distribution of elements between anthophyllite and gedrite is systematic, with gedrite enriched in Al^{IV}, Al^{VI}, Fe^{2+}, Na, Ti, Ca, and Mn and anthophyllite enriched in Si and Mg. The composition limits of orthoamphiboles at this metamorphic grade are controlled by coexistence with phases more enriched in certain elements: the most Si-rich orthoamphiboles coexist with quartz, the most Al-rich with cordierite or staurolite, the most Fe-rich with garnet, the most Mg-rich with talc, chlorite or cordierite, the most Ca-rich with hornblende, and the most Ti-rich with ilmenite or rutile.

Evaluation of published orthoamphibole analyses reveals that the crest of the solvus probably lies at approximately 600±25°C.

Introduction

The existence of a solvus in the orthoamphiboles between low-Al anthophyllite and high-Al gedrite has been noted by Robinson *et al.* (1969, 1970, 1971a), Ross *et al.* (1969), Stout (1969, 1970, 1971, 1972), Spear (1977), and Stoddard (1979).

In the southwestern corner of the Vermont section of the Mt. Cube Quadrangle, New Hampshire and Vermont, the Post Pond Volcanic Member of the Orfordville Formation consists of a variety of rock types that contain coexisting orthoamphiboles. The locality is particularly well suited for a chemographic study of these minerals, because within this one area a highly diverse range of bulk compositions is found, and the entire composition range of orthoamphiboles at this metamorphic grade can be delineated. Moreover, the solvus in the orthoamphiboles from the Mt. Cube Quadrangle shows the widest compositional gap yet reported for these minerals.

This paper describes the textures, mineral chemistry, and phase relations of orthoamphiboles and coexisting minerals from the Post Pond Volcanics with the purpose of (1) outlining the compositional field defined by these minerals, including the limits of the miscibility gap between anthophyllite and gedrite; (2) investigating substitution mechanisms in orthoamphiboles; and (3) estimating the temperature of the crest of the anthophyllite–gedrite solvus.[1]

Geologic setting

The samples were collected from the Post Pond Member of the Orfordville Formation (Hadley, 1942) from the Vermont portion of the southwest corner of the Mt. Cube Quadrangle, New Hampshire and Vermont (see location map, Fig. 1). This unit strikes to

[1] In this paper the names anthophyllite and gedrite are used to describe varieties of orthoamphiboles with $Na(A)+Al^{IV}<1.0$ and $Na(A)+Al^{IV}>1.0$, following the nomenclature of Leake (1978).

0003–004X/80/1112–1103$02.00

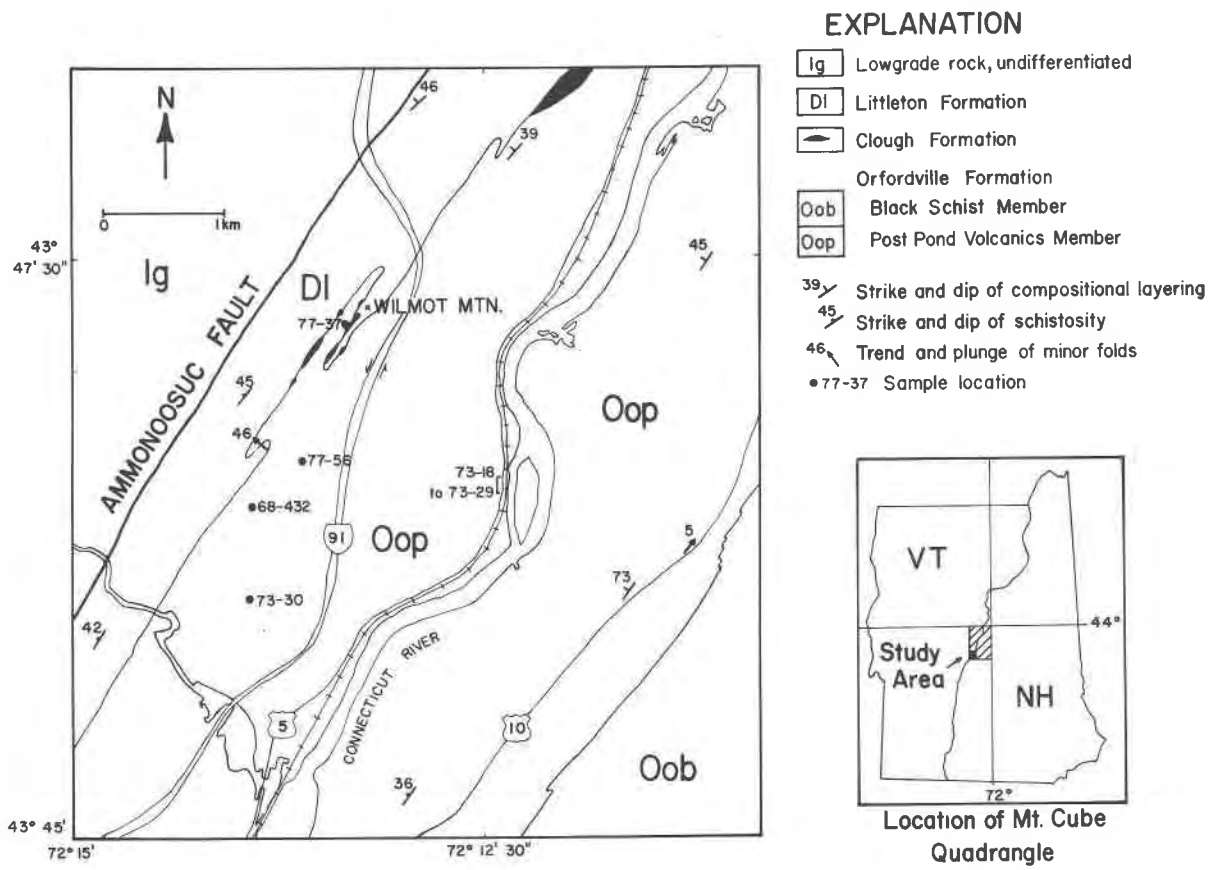

Fig. 1. Geologic map of the southwestern corner of the Mt. Cube Quadrangle, New Hampshire and Vermont, showing the location of the study area. Geology is after Hadley (1942) and Rumble (1969, personal communication).

the northeast and dips to the northwest at 39–73°. To the west, and structurally above the Post Pond Volcanics, are the pelitic schists of the Brick Hill Member of the Orfordville Formation (Hadley, 1942). Rumble (1969) reported quartzite boudins from along the contact between the Post Pond Volcanics and Brick Hill Member, which he interpreted as Silurian Clough Formation, and therefore correlated the Post Pond Volcanics with the middle Ordovician Ammonoosuc Volcanics, which occupy the same stratigraphic position to the east (Thompson *et al.*, 1968).

In the southwest corner of the Mt. Cube Quadrangle, the Post Pond Volcanics are composed of massive to finely bedded mafic to aluminous amphibolites, with minor calc-silicates, biotite gneiss, orthoamphibole gneiss, and cordierite gneiss. There are mafic dikes and agglomerate textures in the rocks exposed in two quarries near Interstate Highway 91, attesting to the original volcanic nature of at least part of this unit. In the roadcut along U.S. Route 5, highly aluminous layers are found, which probably represent volcanic material with an admixture of detritus. To the west, at the upper part of the section, just below the Siluro–Devonian unconformity, there are cordierite and orthoamphibole gneisses high in MgO and low in CaO. The rocks are massive to finely laminated and possibly represent a fossil leached zone or soil horizon at the top of the volcanic pile, or a volcanic sequence that has been hydrothermally altered, possibly by seawater.

Metamorphic grade is in the staurolite–kyanite zone, as shown by abundant staurolite and kyanite in the Brick Hill Member and staurolite in the Post Pond Volcanics. Metamorphic temperatures were estimated with two geothermometers. Oxygen isotope fractionation between quartz and magnetite (1000 $\ln\alpha = 9.8\pm0.11$) yields a temperature of 530±10°C when the calibration of Downs and Deines (1978) is used and 490±10°C when using the calibration of Bottinga and Javoy (1973). The partitioning of Fe and Mg between garnet and biotite yielded a temper-

ature of 535±30°C when compared to the calibration of Ferry and Spear (1978). If one assumes a temperature of 530°C, the presence of kyanite implies a minimum pressure of 4.0 kbar, from the Al_2SiO_5 triple point of Holdaway (1971). The samples were collected from an area approximately 2 km by 1 km and are believed to have been equibrated under approximately isothermal, isobaric conditions.

Textural relations between anthophyllite and gedrite

Orthoamphiboles form large bladed crystals typically 0.1–5.0 mm long, but up to several cm in length in rocks of diverse bulk composition and mineral assemblages (see Table 1). They occur in the foliation plane but also cut across it, indicating that these minerals may have formed late in the crystallization sequence. For comparison, hornblende and cummingtonite from this area almost invariably lie in the foliation.

The orthoamphiboles are distinguished from the clinoamphiboles by their parallel extinction. Anthophyllite is colorless and can be distinguished from Fe-rich gedrite by the moderate pleochroism in gedrite. There is a correlation between the degree of absorption in gedrite and its composition. The strongest pleochroism is observed in Al-, Na-, and Fe-rich gedrites; the weakest in gedrites with high Mg and low Al and Na. In Fe-rich samples the absorption is pale-gray to yellow-gray parallel to α and gray to blue-gray parallel to β and γ (absorption is $\gamma > \beta > \alpha$). In more Mg-rich samples the pleochroism scheme in gedrite is similar, but much weaker. In the most Mg-rich samples [Fe/(Fe+Mg) in anthophyllite ≈0.30], gedrite and anthophyllite are difficult to distinguish on the basis of pleochroism; distinction was made in these samples with the electron microprobe.

Anthophyllite and gedrite coexist in a variety of textures. They occur as discrete grains in some samples, and sharp optical contacts can be seen where the grains touch. They also occur as oriented intergrowths that are optically continuous and exhibit several habits including bladed intergrowths (Fig. 2A), patchy intergrowths, and overgrowths (Fig. 2B). In most occurrences the overgrowth is anthophyllite on gedrite, but in a few samples gedrite overgrowths appear on anthophyllite.

In several samples a lamellar intergrowth of anthophyllite and gedrite is observed (see Figs. 2B, C, D). Lamellae are oriented approximately parallel to (120) and are readily observed in sections cut normal to *c*. In Figures 2B and C the amphibole in the core of the grain is gedrite, whereas anthophyllite makes up the rim. This is the case in most of the samples observed with this intergrowth texture, but in some samples the textural juxtaposition is reversed. Figure 2D shows the distribution of Al between the anthophyllite rim (low Al) and gedrite core (high Al). The (120) lamellae are readily observed in this figure because of the sharp contrast in Al content between the lamellae and the anthophyllite rim. Electron microprobe analysis revealed that the lamellae have approximately the same composition as the core of the grain (*i.e.*, gedrite composition).

The origin of this textural intergrowth is not

Table 1. Representative mineral assemblages of orthoamphibole-bearing rocks from the Post Pond Volcanics

Sample #	Ged**	Anth	Hbld	Cumm	Gar	Stau	Cord	Plag	Qtz	Biot	Naph	Talc	Ch	Ilm	Rut
73-20D	+*	+	+	+	+			An_{32}	x*					x	
73-30I	+	+	+	+				An_{35}	x	x				x	
77-56C	+	+	+	+				An_{33}	x					x	
77-37N	+	+		+	+			An_{29-40}	x	x				x	x
68-432M	+	+	+					An_{33}	x	x			x		x
68-432U	+	+		+				An_{15-29}	x	x					x
68-432D	+	+					+	An_{10-30}	x	x	x	x	x		x
73-29D	+		+		+	+		An_{30}	x	x			x	x	
68-432A	+					+	+	An_{27}	x						x

* The symbol + indicates that an analysis is presented in Tables 2-5. The symbol x indicates the mineral is present but no analysis is presented.

** Abbreviations: Ged=gedrite; Anth=anthophyllite; Hbld=hornblende; Cumm=cummingtonite; Gar=garnet; Stau=staurolite; Cord=cordierite; Plag=plagioclase; Qtz=quartz; Biot=biotite; Naph=Na-phlogopite; Ch=chlorite; Ilm=ilmenite; Rut=rutile.

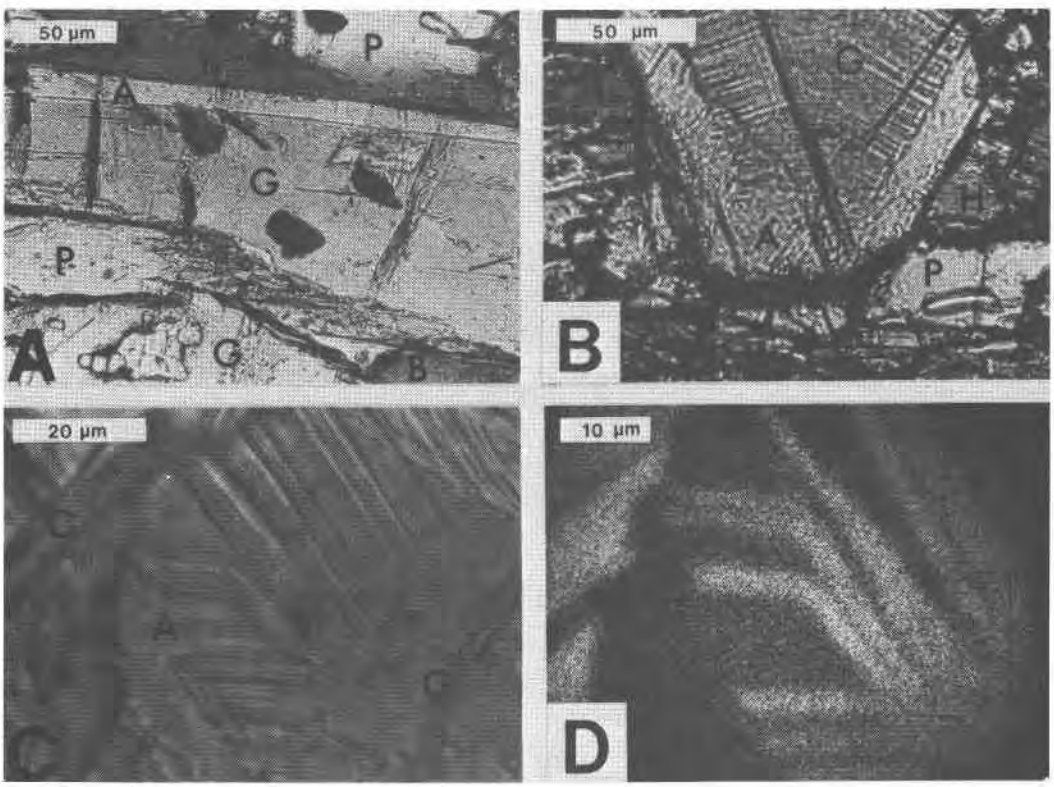

Fig. 2. Photomicrographs and X-ray photograph of anthophyllite–gedrite intergrowths. (A) Bladed intergrowth of anthophyllite and gedrite. (B) Overgrowth of anthophyllite showing (120) lamellar intergrowth texture. (C) Intergrowth of anthophyllite and gedrite showing (120) lamellar intergrowth. Note exsolution lamellae (trending NW–SE) cutting (120) lamellae of gedrite. (D) X-ray photograph (Al$K\alpha$ radiation) for lamellar intergrowth shown in (C). Symbols are G = gedrite, A = anthophyllite, P = plagioclase, H = hornblende, B = biotite, C = chlorite.

known, but it is apparently structurally controlled and related to the growth of the crystals, inasmuch as the lamellae grow normal to the crystal faces and exsolution lamellae cut across the (120) lamellae (see below). It should be noted that not all anthophyllite–gedrite overgrowths exhibit the lamellar texture, but no systematic relation between the presence or absence of lamellar intergrowths and mineral composition could be detected. A similar lamellar intergrowth between anthophyllite and gedrite on a submicroscopic scale was observed by Gittos *et al.* (1976, their Fig. 3) with transmission electron microscopy. In the sample studied by Gittos *et al.* the (120) lamellae resulted from processes related to exsolution.

All grains of coexisting anthophyllite and gedrite exhibit exsolution parallel to (010) (see Figs. 2C and 3); the exsolution is thus most readily observed when viewing sections cut normal to *c*, but can also be observed when viewing sections cut normal to *a*. Exsolution lamellae are less than 1 μm wide and are *always* coarser in gedrite than in coexisting anthophyllite. In some samples, exsolution is present in gedrite whereas the coexisting anthophyllite displays no exsolution (Figs. 2C and 3A). In Figure 3B it can be seen that the exsolution lamellae cut directly across the lamellar texture and are not at all affected by its presence. This observation suggests that the lamellar intergrowth formed before exsolution took place, which is consistent with it having formed during growth of the crystals.

Mineral chemistry

Analytical procedures

Data on representative mineral assemblages are tabulated in Table 1. All chemical analyses were made with an automated MAC electron microprobe either at the Geophysical Laboratory, Carnegie Institution of Washington, or in the Department of Earth and Planetary Sciences, Massachusetts Institute of Technology. Natural and synthetic silicates were

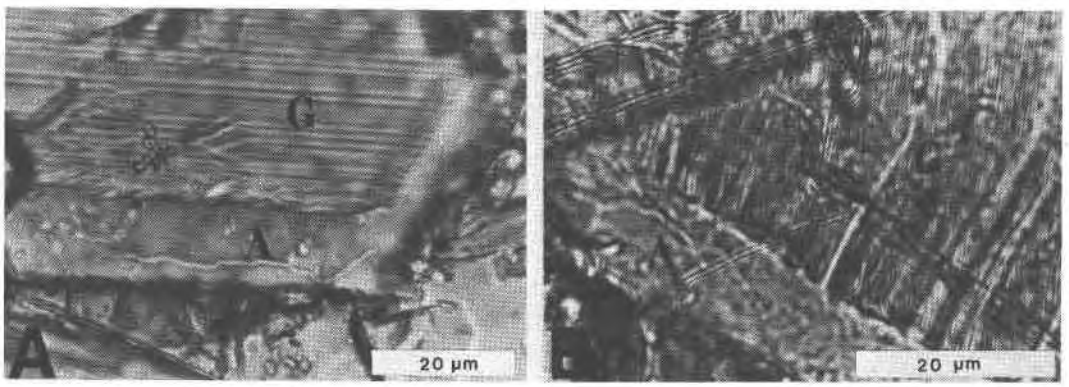

Fig. 3. Photomicrographs showing exsolution features in gedrite and anthophyllite. (A) Exsolution lamellae (the light and dark lines trending E–W) are visible in gedrite but not in anthophyllite. (B) Exsolution lamellae (trending N–S) cut (120) lamellae of gedrite but are not present in anthophyllite. Fig. 3B is the same grain as shown in Fig. 2B. Symbols are G = gedrite, A = anthophyllite.

used as standards; matrix corrections were performed after the procedures of Bence and Albee (1968) using theoretical correction factors (Albee and Ray, 1970). Analyses are estimated to be accurate to within ±3 relative weight % for major elements and ±5 relative weight % for minor elements. Several hundred analyses from over 40 samples were made; representative analyses are presented in Tables 2–5. No K_2O was detected in any analysis of orthoamphibole from the study area (detectability limit ≈0.01 wt.%). Cations were calculated on the anhydrous basis of 23 oxygens. All Fe was assumed to be Fe^{2+} except in hornblende, where Fe^{3+} was calculated from stoichiometric constraints following the procedure in Spear (1980). Cations were assigned to structural positions as follows: all Si and sufficient Al to sum to 8.0 in the tetrahedral site; remaining Al, all Ti, Mg, Fe, Mn, Ca, and sufficient Na to sum to 7.0 in the M_1, M_2, M_3, and M_4 octahedral sites; remaining Na in the alkali site.

Results

Sample 73-29D contains gedrites that are unusually rich in Al_2O_3 and Na_2O, and are characterized by

Table 2. Representative electron microprobe analyses of orthoamphiboles

	73-20D		73-30I		77-56C		77-37N		68-432M		68-432U		68-432D		73-29D	68-432A
	G	A	G	A	G	A	G	A	G	A	G	A	G	A	G	G
								Weight % oxides								
SiO_2	42.80	54.12	46.41	54.43	46.07	55.22	44.83	54.10	47.07	55.42	48.20	55.18	49.17	57.05	40.91	43.44
Al_2O_3	15.52	1.75	14.29	2.35	14.04	2.33	16.81	2.88	14.30	3.46	14.41	4.12	14.11	2.70	19.00	18.08
TiO_2	0.18	0.02	0.16	0.04	0.17	0.04	0.18	0.05	0.17	0.05	0.13	0.05	0.13	0.03	0.18	0.16
MgO	11.73	17.60	15.27	19.85	15.38	20.11	15.63	20.14	16.93	21.08	18.14	21.97	19.90	24.40	11.43	16.15
FeO	25.89	25.36	20.71	21.13	20.09	20.34	18.74	19.82	17.85	18.48	16.14	16.45	14.14	15.22	24.93	17.30
MnO	0.35	0.28	0.36	0.31	0.43	0.42	0.22	0.20	0.25	0.22	0.30	0.30	0.55	0.52	0.17	0.25
CaO	0.47	0.29	0.47	0.36	0.68	0.37	0.45	0.36	0.56	0.39	0.35	0.31	0.24	0.11	0.40	0.29
Na_2O	1.94	0.12	1.73	0.20	1.51	0.13	1.38	0.20	1.74	0.39	1.68	0.38	1.40	0.17	2.38	2.05
	98.88	99.54	99.40	98.67	98.37	98.96	98.24	97.93	98.87	99.49	99.35	98.76	99.64	100.20	99.40	97.72
								Cations per 23 oxygens								
Si	6.346	7.806	6.634	7.767	6.643	7.817	6.417	7.730	6.670	7.725	6.724	7.684	6.767	7.778	6.014	6.239
Al^{IV}	1.654	0.194	1.366	0.233	1.357	0.183	1.583	0.270	1.330	0.275	1.276	0.316	1.233	0.222	1.986	1.761
Al^{VI}	1.059	0.104	1.042	0.162	1.030	0.206	1.254	0.215	1.057	0.293	1.094	0.360	1.054	0.210	1.307	1.300
Ti	0.020	0.002	0.017	0.004	0.018	0.004	0.019	0.005	0.017	0.004	0.014	0.005	0.012	0.001	0.020	0.017
Mg	2.592	3.783	3.253	4.222	3.305	4.242	3.334	4.288	3.576	4.382	3.771	4.559	4.084	4.958	2.504	3.457
Fe	3.210	3.059	2.476	2.522	2.423	2.408	2.243	2.368	2.112	2.152	1.883	1.916	1.624	1.732	3.065	2.078
Mn	0.044	0.034	0.044	0.037	0.053	0.050	0.027	0.024	0.029	0.024	0.035	0.035	0.061	0.056	0.021	0.030
Ca	0.075	0.045	0.072	0.055	0.105	0.056	0.069	0.055	0.083	0.057	0.052	0.046	0.032	0.016	0.063	0.045
Na(M4)	0.0	0.0	0.096	0.0	0.006	0.034	0.054	0.025	0.126	0.088	0.151	0.079	0.133	0.027	0.020	0.073
Na(A)	0.558	0.034	0.384	0.055	0.356	0.002	0.329	0.030	0.352	0.014	0.303	0.024	0.239	0.017	0.658	0.498
Fe/Fe+Mg	0.553	0.447	0.432	0.374	0.423	0.362	0.402	0.356	0.371	0.329	0.333	0.296	0.285	0.259	0.550	0.373

Table 3. Representative electron microprobe analyses of hornblende

	73-20D	73-30I	77-56C	68-432M	73-29D
	Weight % oxides				
SiO_2	42.66	45.04	43.63	45.22	41.08
Al_2O_3	16.30	16.82	16.29	15.43	17.98
TiO_2	0.45	0.53	0.42	0.42	0.37
MgO	8.45	10.88	10.89	12.16	7.46
FeO	18.86	13.60	14.64	13.07	18.85
MnO	0.12	0.15	0.18	0.11	0.11
CaO	10.23	10.50	10.30	10.39	10.15
Na_2O	1.75	1.85	1.73	2.10	1.98
K_2O	0.19	0.21	0.16	0.14	0.24
	99.01	99.58	98.24	99.04	98.22
	Cations per 23 oxygens				
Si	6.200	6.355	6.262	6.399	6.040
Al^{IV}	1.800	1.645	1.738	1.601	1.960
Al^{VI}	0.993	1.153	1.018	0.973	1.157
Ti	0.049	0.056	0.045	0.045	0.041
Fe^{3+}*	0.635	0.422	0.608	0.503	0.583
Mg	1.830	2.288	2.329	2.564	1.635
Fe^{2+}	1.657	1.182	1.150	1.044	1.735
Mn	0.015	0.018	0.022	0.013	0.014
Ca	1.593	1.587	1.584	1.575	1.599
Na(M4)	0.228	0.294	0.244	0.283	0.236
Na(A)	0.265	0.212	0.237	0.293	0.329
K	0.035	0.038	0.029	0.025	0.045
ΣA	0.300	0.250	0.266	0.318	0.374
$Fe^{3+}/Fe^{3+}+Mg$	0.277	0.263	0.346	0.325	0.252
$Fe^{2+}/Fe^{2+}+Mg$	0.475	0.341	0.331	0.289	0.515

* Fe^{3+} determined from stoichiometry

a very strong blue-gray pleochroism. They are slightly less aluminous (Al_2O_3 = 19.00 to 19.11 wt.%) than a gedrite reported by Robinson and Jaffe (1969, sample I34I; Al_2O_3 = 19.81%). The Na_2O content of these gedrites, however, is greater (2.27 to 2.38 wt.%) than that of sample I34I (Na_2O = 1.92%). The aluminian ferroanthophyllite reported by Seki and Yamasaki (1957) has Al_2O_3 and Na_2O contents of 19.47–19.72 wt.% and 1.08–1.16 wt.%, respectively. To my knowledge, the gedrites from sample 73-29D have the highest Na_2O content of any orthoamphiboles reported in the literature (*cf.*, Rabbitt, 1948; Robinson and Jaffe, 1969; Robinson *et al.*, 1971a; Lal and Moorhouse, 1969; Gable and Sims, 1970). These highly aluminous gedrites coexist with staurolite, which is the most Al-rich phase to coexist with gedrite at these metamorphic conditions (staurolite–kyanite zone).

The major chemical variations in orthoamphiboles can be described in terms of end-member anthophyllite [$Mg_7Si_8O_{22}(OH)_2$] plus three substitution mechanisms: Fe ⇆ Mg (Fe–Mg exchange), $Al^{VI}Al^{IV}$ ⇆ MgSi (tschermak exchange) and $NaAl^{IV}$ ⇆ □ Si (edenite exchange). Other substitutions, such as those involving Mn, Ti, Fe^{3+}, or Ca are of minor importance.

Gedrite differs from anthophyllite primarily in the amount of edenite and tschermak substitutions: the miscibility gap between these two minerals represents a discontinuity in the amount of these two substitutions. Deer, Howie and Zussman (1963, p. 214) report an end-member formula for gedrite of $Mg_5Al_2^{VI}Al_2^{IV}Si_6O_{22}(OH)_2$, but Robinson *et al.* (1971a) have emphasized the importance of Na in the A site of gedrite and have postulated an ideal end-member gedrite composition of

$$Na_{0.5}(Mg,Fe^{2+})_2(Mg,Fe^{2+})_{3.5}Al_{1.5}Si_6Al_2O_{22}(OH)_2$$

based on evaluation of all available wet-chemical analyses. This formula represents a combination of the edenite and tschermak substitution in a ratio of one to three. Figure 4 is a plot of A-site occupancy *vs.* Al^{IV} for gedrites and anthophyllites from the study area. Only selected coexisting pairs have been shown for the sake of clarity. The trend from anthophyllite to gedrite is very pronounced and is, in general, towards the composition of "ideal" gedrite as defined

Table 4. Representative electron microprobe analyses of cummingtonite

	73-20D	73-30I	77-56C	77-37N	68-432U
	Weight % oxides				
SiO_2	53.84	56.04	55.32	55.51	57.15
Al_2O_3	1.61	0.90	1.00	1.03	1.18
TiO_2	0.01	0.01	0.02	0.0	0.02
MgO	17.44	19.56	20.04	20.24	21.99
FeO	25.63	21.91	20.75	20.82	18.09
MnO	0.19	0.37	0.40	0.23	0.29
CaO	0.41	0.51	0.54	0.38	0.38
Na_2O	0.15	0.02	0.02	0.04	0.07
	99.28	99.32	98.09	98.25	99.16
	Cations per 23 oxygens				
Si	7.802	7.954	7.923	7.927	7.964
Al^{IV}	0.198	0.046	0.077	0.073	0.036
Al^{VI}	0.077	0.105	0.092	0.100	0.158
Ti	0.001	0.001	0.002	0.0	0.002
Mg	3.767	4.138	4.277	4.308	4.568
Fe	3.106	2.601	2.485	2.487	2.109
Mn	0.023	0.044	0.049	0.028	0.034
Ca	0.064	0.078	0.083	0.058	0.057
Na	0.042	0.006	0.006	0.011	0.019
Σ	15.080	14.973	14.994	14.992	14.947
Fe/Fe+Mg	0.452	0.386	0.367	0.366	0.316

Table 5. Representative electron microprobe analyses of garnet, staurolite, and cordierite

	Garnet			Staurolite		Cordierite	
	73-20D	77-37N	73-29D	68-432A	73-29D	68-432D	68-432A
	Weight % oxides						
SiO_2	37.11	39.16	38.55	27.88	27.51	51.20	49.68
Al_2O_3	21.46	21.38	21.51	52.81	52.15	33.43	32.84
TiO_2	0.08	0.01	0.0	0.67	0.50	0.0	0.0
MgO	4.11	5.55	4.15	2.79	2.33	11.77	11.14
FeO	34.39	30.67	34.57	12.74	14.45	2.70	3.52
MnO	0.82	1.13	0.58	0.14	0.06	0.05	0.05
ZnO	n.d.*	n.d.	n.d.	0.43	1.25	n.d.	n.d.
CaO	2.72	2.86	2.79	0.0	0.0	0.02	0.0
Na_2O	0.05	0.0	n.d.	0.0	0.0	0.12	0.16
	100.73	100.76	102.18	97.46	98.25	99.30	97.39
	Cations						
	12 oxygens			46 oxygens		18 oxygens	
Si	2.953	3.050	3.009	7.753	7.692	5.074	5.047
Al	2.013	1.963	1.979	17.315	17.189	3.905	3.936
Ti	0.005	0.001	0.0	0.140	0.105	0.0	0.0
Mg	0.487	0.644	0.483	1.157	0.971	1.736	1.687
Fe	2.289	1.998	2.257	2.964	3.379	0.224	0.299
Mn	0.055	0.075	0.038	0.033	0.015	0.002	0.004
Zn	n.d.	n.d.	n.d.	0.088	0.258	n.d.	n.d.
Ca	0.232	0.239	0.233	0.0	0.0	0.001	0.0
Na	0.002	0.0	n.d.	0.0	0.0	0.023	0.032
Σ	8.037	7.970	8.004	29.450	29.608	10.964	11.005
Fe/Fe+Mg	0.824	0.756	0.824	0.719	0.777	0.114	0.151

* n.d. means not determined

by Robinson *et al.* There is considerable fanning of the tie lines, however; this represents real differences in the A-site occupancy between different mineral pairs. In general, the more Mg-rich pairs have the lower A-site occupancies, as can be seen in Figure 5. Thus the notion of a linear trend from anthophyllite to "ideal" gedrite must be modified to include variations in Fe/Mg. The apparent tendency of hornblende-absent assemblages to have relatively low A-site occupancies reflects the low Fe/Mg content of these samples (see Fig. 5) rather than a crystal-chemical effect caused by low CaO contents.

The miscibility gap between anthophyllite and gedrite can be clearly seen in Figures 4, 5, 6, and 7. It is manifested by a large discontinuity in the A-site occupancy and in the Al^{VI} and Al^{IV} contents; that is, along the edenite and tschermakite substitution directions.

A-site occupancy in anthophyllite ranges from approximately 0.0 to 0.1 cations; in coexisting gedrite these values range from 0.25 to 0.55. Values of Al^{VI} range from 0.36 to 0.10 in anthophyllite and 1.24 to 0.92 in gedrite; Al^{IV} is 0.2±0.1 in anthophyllite and 1.4±0.2 in gedrite. Some of the scatter in maximum

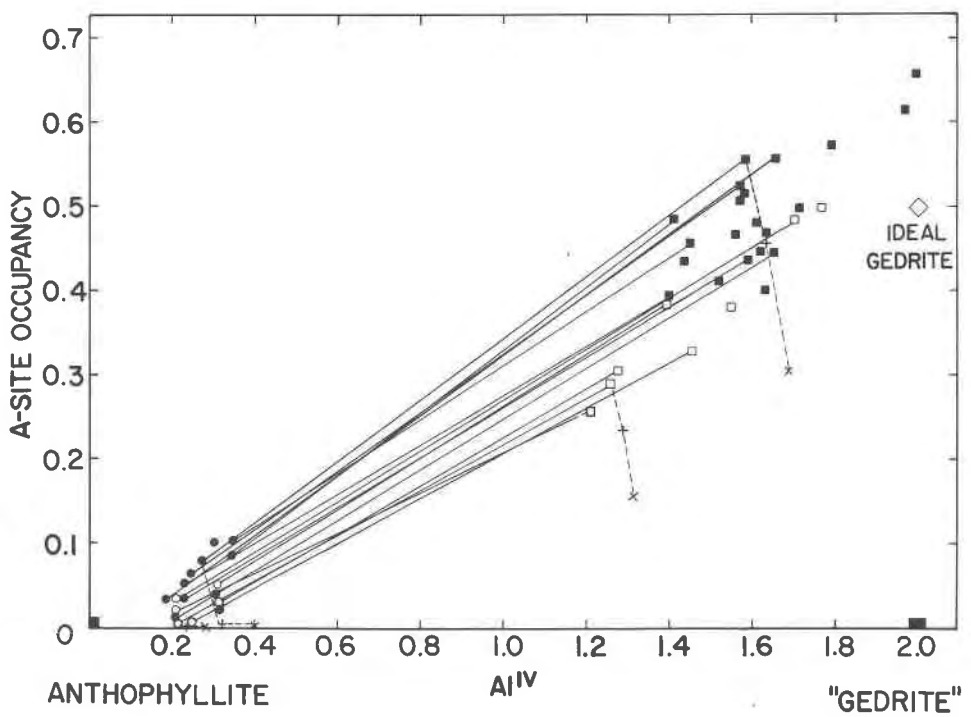

Fig. 4. Plot of A-site occupancy *vs.* Al^{IV} in gedrite (squares) and anthophyllite (circles). Tielines connect coexisting phases. Filled symbols are for samples containing hornblende; open symbols are for samples without hornblende. The symbols "+" and "×" indicate plotting positions of gedrite and anthophyllite (connected by dashed line) with $Fe^{3+}/(Fe^{3+} + Fe^{2+})$ calculated at 10% and 25%, respectively.

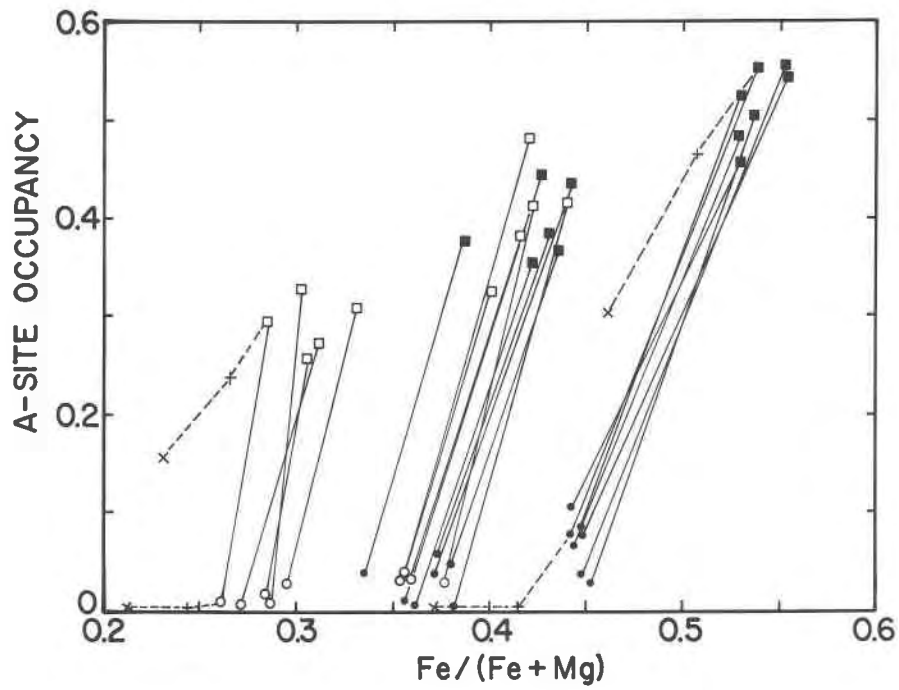

Fig. 5. A-site occupancy *vs.* Fe/(Fe+Mg) for coexisting anthophyllite and gedrite. Symbols as in Fig. 4.

and minimum Al content of gedrite and anthophyllite is brought about because of the pervasive exsolution and the difficulty in measuring the bulk Al content of phases containing exsolution lamellae. The above values of A-site occupancy, Al^{VI}, and Al^{IV} encompass the range in composition for *coexisting* gedrite and anthophyllite only. Orthoamphiboles not constrained to lie on the solvus can have compositions outside of this range. There is a slight tendency for Mg-rich orthoamphiboles to be enriched in Al^{VI} (Fig. 6); there is a strong tendency for Fe-rich orthoamphiboles to be enriched in A-site occupancy (Fig. 5). Moreover, the size of the miscibility gap, as expressed by A-site occupancy, increases with increasing Fe/(Fe+Mg).

The effect of ferric iron content on recalculated orthoamphibole formulae warrants discussion. Wet-chemical analyses of orthoamphiboles from similar rocks (Robinson and Jaffe, 1969; Rabbitt, 1948) contain less than 3.0 wt.% Fe_2O_3 or $Fe^{3+}/(Fe^{3+} + Fe^{2+})$ less than 0.15, although Lal and Moorhouse (1969) report gedrite analyses with $Fe^{3+}/(Fe^{3+} + Fe^{2+})$ as high as 0.25. If some of the iron in the orthoamphiboles is recalculated as Fe^{3+}, the resulting structural formula shows higher values for Al^{IV} and lower values for Al^{VI}, A-site occupancy, and $Fe^{2+}/(Fe^{2+} + Mg)$ than the same analysis calculated with all iron as Fe^{2+}. Coexisting anthophyllite and gedrite from an iron-rich bulk composition and a magnesium-rich bulk composition have been recalculated, assuming 10% and 25% ferric iron in each phase. The results are indicated in Figures 4–7 by the (+) and (×) symbols connected by dashed lines to the respective orthoamphibole. If comparable amounts of Fe^{3+} are present in Fe- and Mg-rich gedrites, then the increase in A-site occupancy with increasing $Fe^{2+}/(Fe^{2+} + Mg)$ observed in Figures 4 and 5 is still present. However, if gedrites from Fe-rich bulk composition are preferentially enriched in Fe^{3+} over gedrites from Mg-rich bulk compositions, then some or all of this variation will disappear. In fact, it is possible to choose ferric iron contents so that all recalculated gedrites will have the same A-site occupancy, or alternatively so that all gedrites and anthophyllites plot on a linear trend, as has been noted by Robinson *et al.* (1971a). It is unlikely that all gedrites have identical A-site occupancies; this would require the most iron-rich gedrites to have 15–25% Fe^{3+} and the most magnesium-rich gedrites to have 0%. If this were the case, however, the relationship between Al^{IV} and $Fe^{2+}/(Fe^{2+} + Mg)$ and Al^{VI} and $Fe^{2+}/(Fe^{2+} + Mg)$ would still be present and even accentuated (see Figs. 6 and 7). If all gedrites and anthophyllites were recalculated to fall on a single line in Figure 4, system-

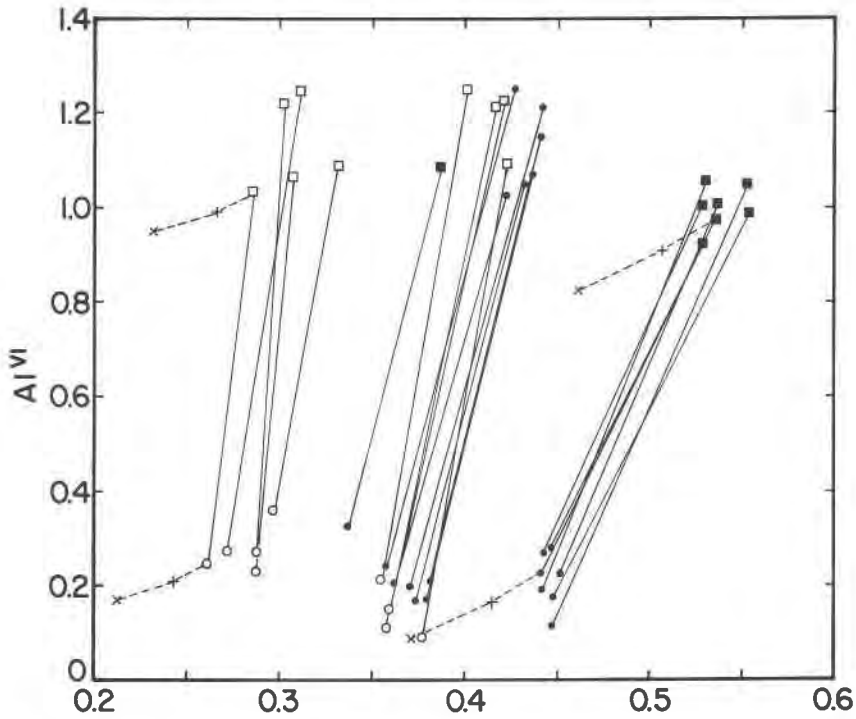

Fig. 6. Al^{VI} *vs.* Fe/(Fe+Mg) for coexisting anthophyllite and gedrite. Symbols as in Fig. 4.

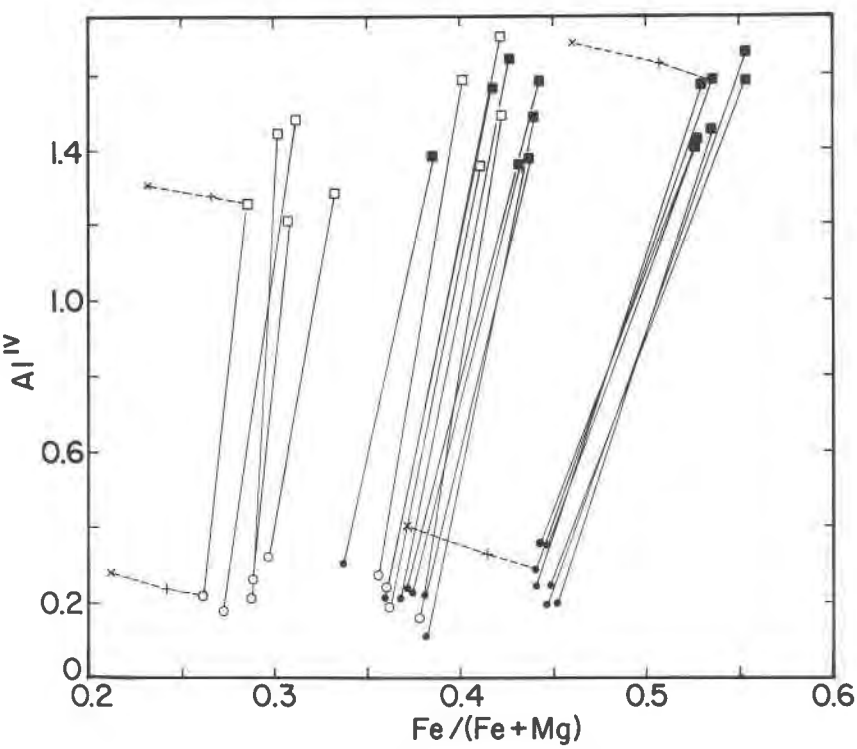

Fig. 7. Al^{IV} *vs.* Fe/(Fe+Mg) for coexisting anthophyllite and gedrite. Symbols as in Fig. 4.

atic oxidation of Fe-rich samples would still be required. Moreover, the relationship between $Fe^{2+}/(Fe^{2+} + Mg)$ and A-site occupancy (Fig. 5), Al^{VI} (Fig. 6), and Al^{IV} (Fig. 7) would still be present.

No petrographic or chemical evidence for the systematic oxidation of Fe-rich samples, such as the presence of hematite or of considerable Fe_2O_3 component in ilmenite, has been observed. Although the question of ferric iron in the orthoamphibole must remain unresolved, it is believed that much of the variation of A-site occupancy, Al^{VI}, and Al^{IV} with $Fe^{2+}/(Fe^{2+} + Mg)$ observed in Figures 4–7 represents real crystal chemical differences between iron-rich and magnesium-rich samples.[2]

The miscibility gap depicted in Figures 4–7 for the orthoamphiboles is the widest gap reported for these minerals, as will be discussed later. Note that the so-called miscibility gap between actinolite and hornblende, which are the monoclinic calcic amphibole equivalents of anthophyllite and gedrite, is in the same composition direction and spans approximately the same gap (*e.g.*, Klein, 1969; Brady, 1974).

The distribution of the edenite and tschermakite components between anthophyllite and gedrite can be seen in Figure 8. The definitions of K_D are as follows:

$$K_D^{Eden} \equiv \left[\frac{Na(A)}{\square(A)}\right]_{ged} \Big/ \left[\frac{Na(A)}{\square(A)}\right]_{anth} \quad \text{and}$$

$$K_D^{Tsch} \equiv \left[\frac{Al^{VI}}{Mg\ (M2)}\right]_{ged} \Big/ \left[\frac{Al^{VI}}{Mg\ (M2)}\right]_{anth}$$

where $\square$ refers to a vacancy in the A site. The values of $\ln K_D^{Tsch}$ are approximately 2.5±0.75 and, except for some erratic points, those for $\ln K_D^{Eden}$ cluster around 2.8±0.5. The points on the $\ln K_D^{Eden}$ plot with values of infinity are for anthophyllites with 0.0 calculated A-site occupancy, although these amphiboles do contain measurable Na_2O. Because of the great uncertainties in calculating A-site occupancies, the values of $\ln K_D^{Eden}$ should be considered only approximate. Most importantly, however, there is no systematic variation in K_D^{Eden} or K_D^{Tsch} with Fe/(Fe+Mg).

The distribution of Fe and Mg between coexisting anthophyllite and gedrite can be seen in Figures 5, 6, and 7, where Fe/(Fe+Mg) has been plotted against

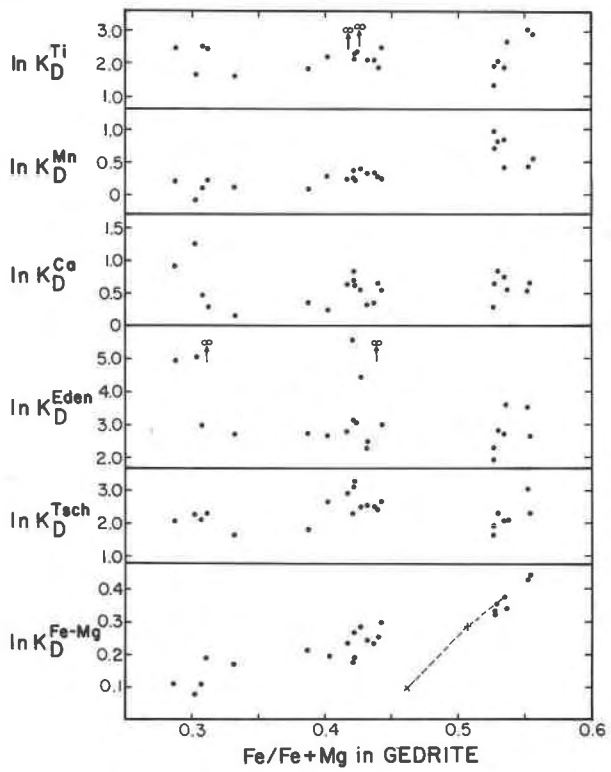

Fig. 8. $\ln K_D$ *vs.* Fe/(Fe+Mg) for coexisting anthophyllite–gedrite. K_D for each plot is different and is defined in text. The symbols "+" and "×" indicate change in $\ln K_D^{Fe-Mg}$ if gedrite is recalculated assuming $Fe^{3+}/(Fe^{3+} + Fe^{2+}) = 0.10$ and 0.25, respectively. The symbol "∞" with the arrow indicates that a point plots at infinity.

A-site occupancy, Al^{VI}, and Al^{IV}. Gedrite is always enriched in Fe relative to coexisting anthophyllite. Moreover, the partitioning is a function of Fe/Mg ratio: gedrite is more enriched in Fe relative to anthophyllite in the Fe-rich than in the Fe-poor bulk compositions. Values of $\ln K_D^{Fe-Mg}$ [$K_D^{Fe-Mg} = (Fe/Mg)_{ged}/(Fe/Mg)_{anth}$] range from 0.38±0.05 in the most Fe-rich sample to 0.13±0.05 in the most Fe-poor samples. The trend of increasing K_D with increasing Fe/Mg is still apparent if Fe-rich gedrites are recalculated assuming 10% Fe^{3+}; the trend only disappears if Fe-rich gedrites contain 25% Fe^{3+} and Fe-poor gedrites contain 0% (see Fig. 8).

Figure 9 shows plots of total Fe *vs.* Al^{VI} and Mg *vs.* Al^{VI} for coexisting gedrite and anthophyllite. Assumptions about Fe^{3+} in the orthoamphiboles affect this diagram very little. The plots show that total Fe varies very little between anthophyllite and coexisting gedrite, whereas anthophyllite is always enriched in Mg relative to gedrite. Furthermore, there is an

[2] Mössbauer spectra of an Fe-rich gedrite [Fe/(Fe+Mg) = 0.48] and an Mg-rich gedrite [Fe/(Fe+Mg) = 0.28] reveal that both orthoamphiboles have $Fe^{3+}/(Fe^{3+} + Fe^{2+})$ ratios of less than 0.05, thus substantiating the observed trends with respect to Fe/(Fe+Mg).

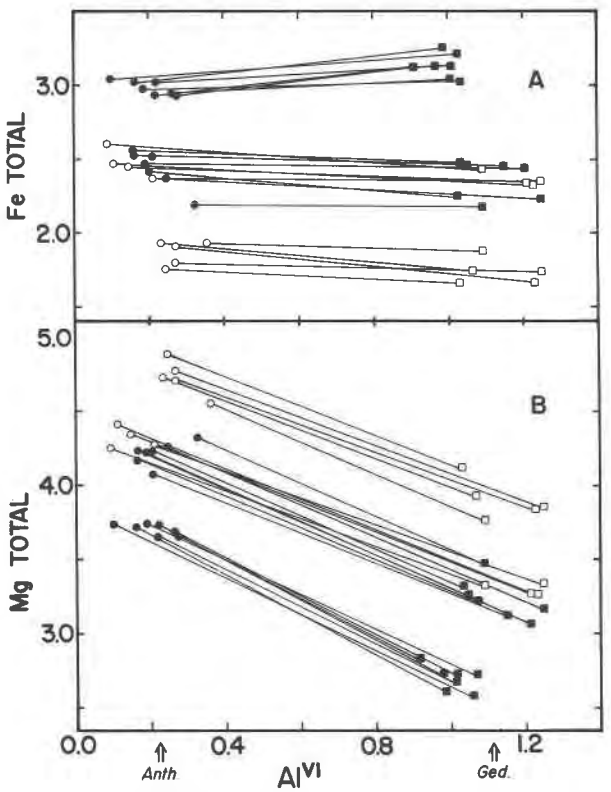

Fig. 9. Total Fe *vs.* Al^{VI} and (B) total Mg *vs.* Al^{VI} for coexisting anthophyllite (circles) and gedrite (squares).

approximately 1:1 inverse relation between the Mg and Al^{VI} contents of coexisting gedrite and anthophyllite. The implication of this relation is that the tschermak exchange reaction ($Al^{VI}Al^{IV} \rightleftarrows MgSi$) involves only the Mg-end member component in orthoamphiboles. A similar relation in the orthoamphiboles has been described by Stout (1972, personal communication), Abraham and Schreyer (1973), and Kamineni (1975), and the implications for exsolution mechanisms are discussed by Robinson *et al.* (1971a, p. 1030–1031). Octahedral Al is highly concentrated in the M2 site of aluminous orthoamphiboles and, relative to Fe, Mg partitions strongly into this site (Finger, 1970; Papike and Ross, 1970).[3] The relationship depicted in Figure 9 is consistent with these site-occupancy assignments and with the notion that the tschermak exchange in orthoamphiboles involves primarily the M2 octahedral site (in addition to tetrahedral sites to maintain charge balance).

The distribution of Ti, Mn, and Ca between anthophyllite and gedrite can be seen in Figures 8, 10, 11, and 12. Ti is always enriched in gedrite relative to anthophyllite: typical values for anthophyllite range from 0.02 to 0.07 wt.% and for gedrite from 0.12 to 0.20 wt.%. There is a tendency for Fe-rich orthoamphiboles (especially gedrite) to contain more Ti than Mg-rich orthoamphiboles (see Fig. 10). All assemblages contain a phase enriched in TiO_2: rutile in Mg-rich samples and ilmenite in Fe-rich samples (Fig. 10).

Values of $\ln K_D^{Ti}$ $\{K_D^{Ti} \equiv [Ti/Mg\ (M2)]_{ged}/[Ti/Mg\ (M2)]_{anth}\}$ cluster around 2.2±0.08 (except for two erratic points representing anthophyllite with no measured TiO_2; see Fig. 8). There is no systematic variation in $\ln K_D^{Ti}$ with Fe/(Fe+Mg).

The distribution of Ca between anthophyllite and gedrite (Fig. 11) is systematic: gedrite is always en-

[3] Papike and Ross show similar distributions of $Fe^* = Fe^{2+} + Fe^{3+} + Mn + Ti$ and Mg among the M1, M2, and M3 sites of gedrite. If it is assumed that Fe^{3+} and Ti are located exclusively in the M2 site, then calculations reveal that Mg is greatly enriched in the M2 site relative to Fe^{2+}.

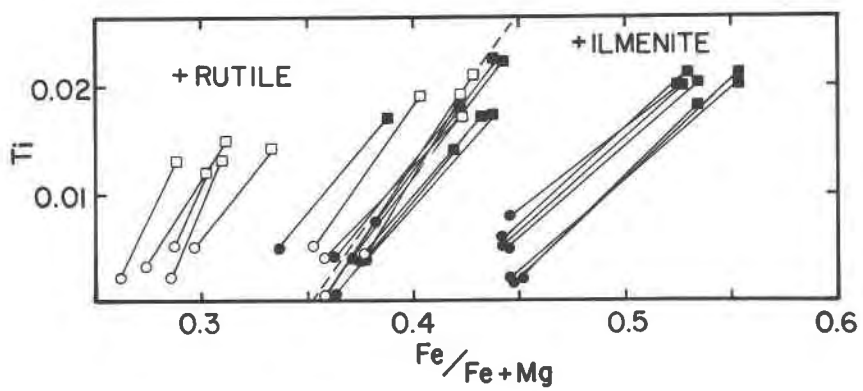

Fig. 10. Ti *vs.* Fe/(Fe+Mg) for coexisting anthophyllite and gedrite. Symbols as in Fig. 4. Dashed line separates the assemblages containing rutile from assemblages containing ilmenite.

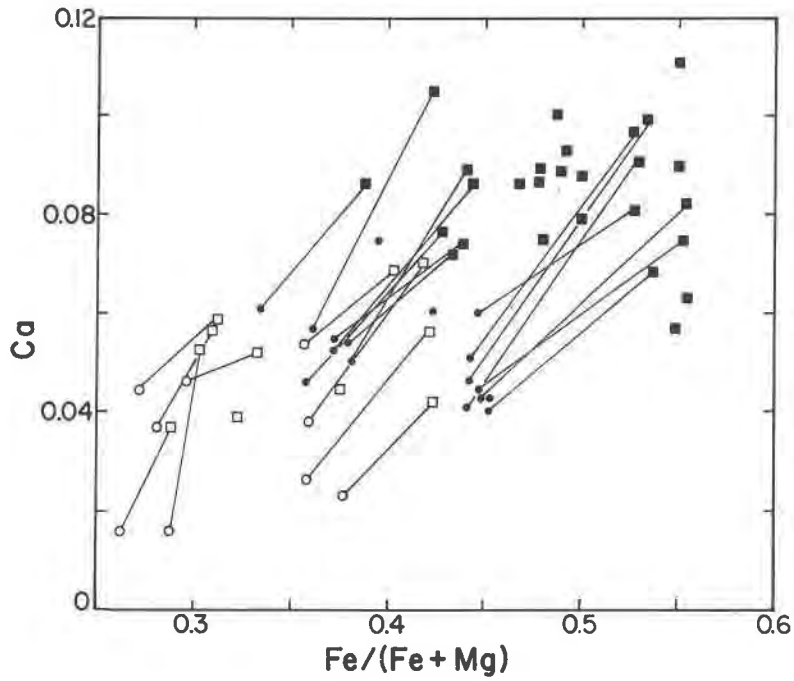

Fig. 11. Ca *vs.* Fe/(Fe+Mg) for coexisting anthophyllite (circles) and gedrite (squares). Symbols as in Fig. 4.

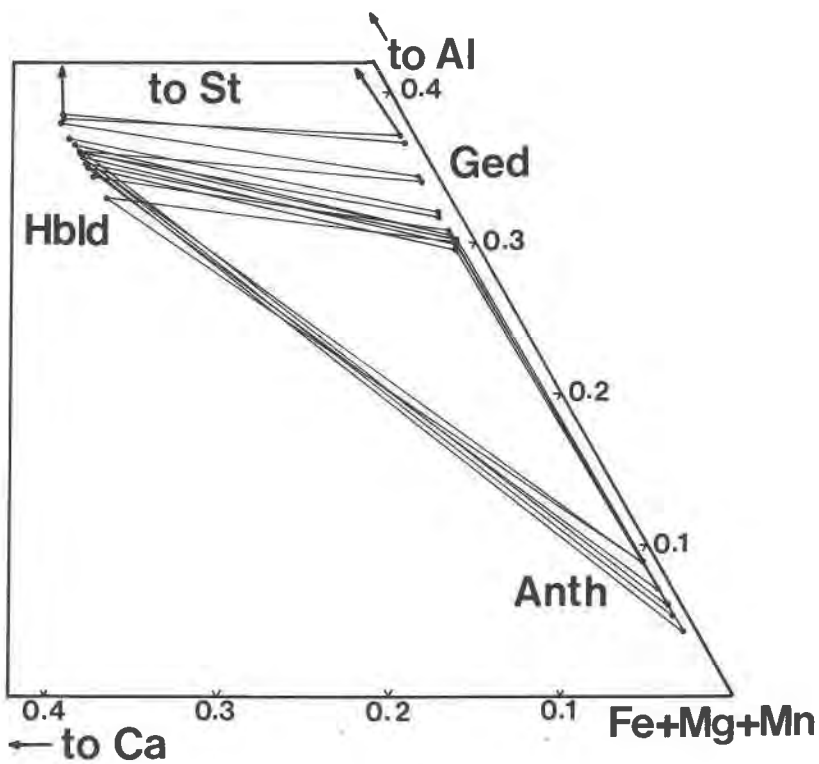

Fig. 12. Portion of the compositional triangle Al–Ca–(Fe+Mg+Mn) showing compositions of analyzed anthophyllites (Anth), gedrites (Ged), and hornblendes (Hbld). Tielines connect coexisting phases. Hornblende is the most Ca-rich phase in these rocks; the plot displays the maximum solubility of Ca in orthoamphiboles at this metamorphic grade. The most Al-rich gedrites and hornblendes coexist with staurolite (St), which is the most aluminous phase for Fe-rich assemblages in these rocks.

riched in Ca relative to anthophyllite. The amount of Ca in the orthoamphibole is a function of bulk CaO content. The hornblende-containing assemblages (closed symbols) show relatively systematic Ca contents in both gedrite and anthophyllite. Orthoamphiboles in hornblende-absent assemblages (open symbols) show erratic CaO contents and values lower than those in hornblende-containing assemblages. The distribution of Ca as well as Al between hornblende and orthoamphiboles can also be seen in Figure 12, which illustrates that Ca contents in hornblende, gedrite, and anthophyllite are very consistent for all assemblages. The crossing tielines result from the condensation of Fe+Mg+Mn into one component.

Distribution of Ca between orthoamphibole pairs $\{K_D^{Ca} \equiv [Ca/(Fe,M4 + Mn,M4)]_{ged}/[Ca/(Fe,M4 + Mn,M)]_{anth}\}$ shows no dependency on Fe/(Fe+Mg) (see Fig. 8). Values of $\ln K_D^{Ca}$ cluster around 0.6±0.4.

The Mn contents of gedrite and anthophyllite are small (0.09–0.55 wt.%) and depend largely on bulk MnO content. Mn favors gedrite over anthophyllite in all but three samples. Values of $\ln K_D^{Mn}$ $\{K_D^{Mn} \equiv [Mn/(Mn+Fe+Mg)]_{ged}/[Mn/(Mn+Fe+Mg)]_{anth}\}$ increase with increasing Fe/(Fe+Mg) from 0.1±0.15 at Fe/(Fe+Mg) = 0.3 to 0.7±0.3 at Fe/(Fe+Mg) = 0.55 (see Fig. 8).

The composition of orthoamphiboles and coexisting minerals are displayed in a plot of Al–Fe–Mg in Figure 13. This diagram is not a projection of the phase relations, and crossing tielines should not be construed as indicative of reaction relations. The plot is presented to show the compositional limits of orthoamphiboles with respect to Al, Fe, and Mg. Orthoamphiboles with the highest Fe/(Fe+Mg) are found in association with garnet. Gedrite and anthophyllite coexisting with garnet have Fe/(Fe+Mg) ratios of 0.53–0.55 and 0.44–0.46, respectively, and gedrite coexisting with garnet and staurolite has a Fe/(Fe+Mg) ratio of 0.55.

The most Mg-rich orthoamphiboles from this grade are found coexisting with talc, chlorite, and/or cordierite, all of which are present in sample 68-432D.

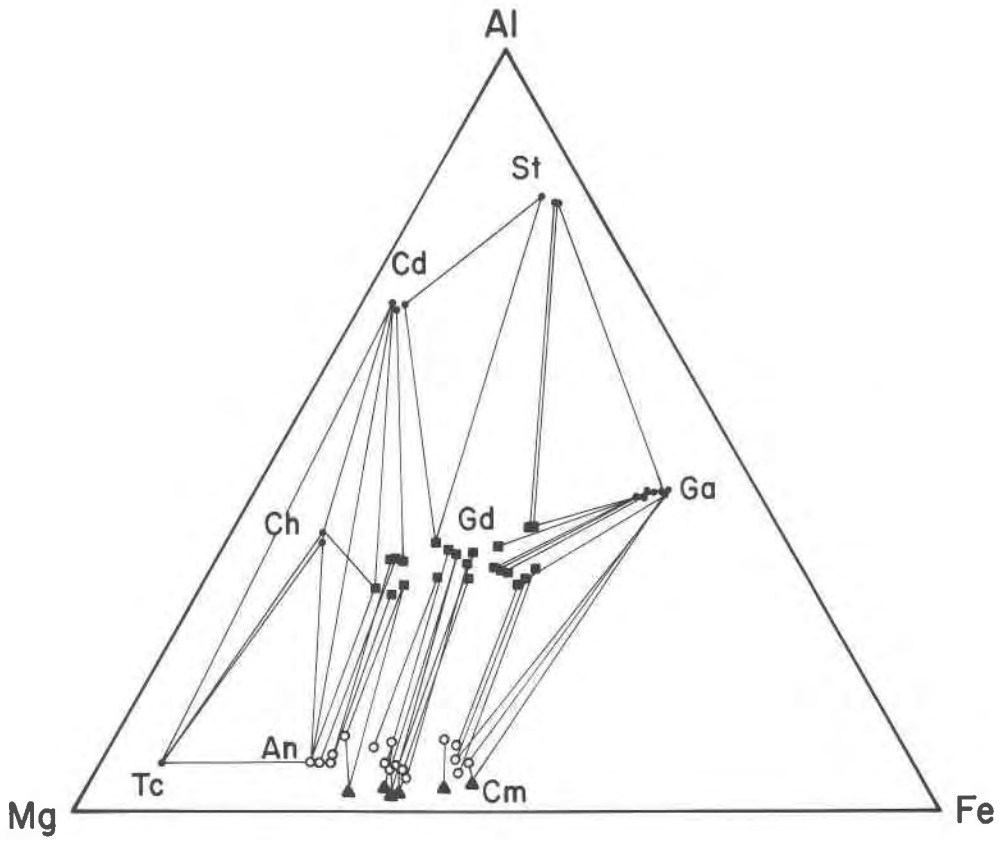

Fig. 13. Al–Fe–Mg compositional plane showing compositions of analyzed gedrite (squares), anthophyllite (open circles), cummingtonite (triangles), garnet (Ga), staurolite (St), cordierite (Cd), chlorite (Ch), and talc (Tc). This figure reveals the limits of the solubility of Al, Fe, and Mg in orthoamphiboles at the metamorphic grade of the Post Pond Volcanics.

The most aluminous anthophyllites coexist with gedrite and the most aluminous gedrites coexist with staurolite (in Fe-rich samples, see also Fig. 12) or cordierite (in Mg-rich samples). The Al-poor limit for gedrite is defined by coexistence with anthophyllite and for anthophyllite by coexistence with cummingtonite.

Discussion

The miscibility gap between anthophyllite and gedrite has been discussed by Robinson *et al.* (1969, 1970, 1971a), and Ross *et al.* (1969), who analyzed exsolution textures in super-solvus orthoamphiboles, and Stout (1969, 1970, 1971, 1972), Spear (1977) and Stoddard (1979, personal communication), who analyzed coexisting sub-solvus orthoamphiboles. From the compositional data and estimates of metamorphic temperatures in these studies combined with data from the present study, it is possible to construct a hypothetical T–X solvus for the orthoamphiboles.

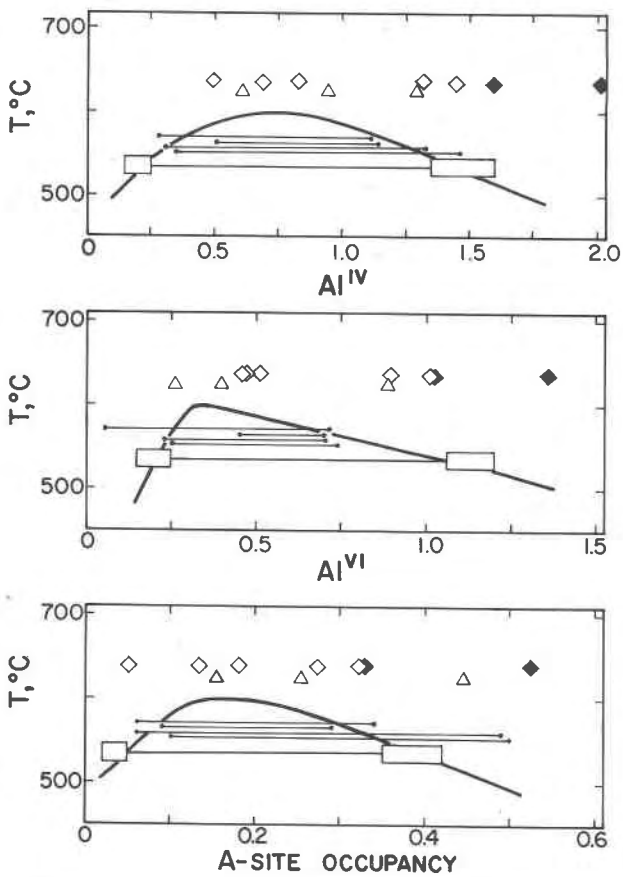

Fig. 14. Hypothetical T–X solvus for orthoamphiboles drawn at $Fe^{2+}/(Fe^{2+}+Mg) \approx 0.4$, based on data from this study (large boxes), Stout (1970, 1972) (circles), James *et al.* (1978) (triangles), and Robinson *et al.* (1971a) (diamonds). Filled diamonds are orthoamphiboles from Robinson *et al.* showing no exsolution. Temperature estimates are discussed in text.

In Figure 14 the solvus is drawn as a function of A-site occupancy, Al^{VI} and Al^{IV}. The lowest temperature data, and the data that record the widest miscibility gap, are from this study. The data from Stout (1970, 1972) are from the Telemark region, Norway, where metamorphic conditions are in the kyanite–sillimanite zone. Spear (1977, 1978) has estimated that the Telemark amphibolites have crystallized at a higher T or lower P_{H_2O} than the Post Pond Volcanics. A single pair of coexisting garnet + cordierite from Stout (1972) yields temperatures of 553° and 570°C using the calibrations of Thompson (1976) and Holdaway and Lee (1977), respectively. Individual pairs of coexisting anthophyllite + gedrite from Stout (1972) have been plotted on Figure 14, assuming a temperature of 560° with an estimated error of ±25°C. On the average, these data show a smaller miscibility gap than data from the Post Pond Volcanics, although there are some notably discrepant points.

James *et al.* (1978) and Robinson *et al.* (1971a) present orthoamphibole analyses that completely bridge the solvus. James *et al.* estimated metamorphic conditions at 625°C, 3–6 kbar; Tracy *et al.* (1976) estimated that the samples studied by Robinson *et al.* crystallized at 625–650°C, ~6 kbar. Note that the most Al- and Na-rich gedrites studied by Robinson *et al.* do not display exsolution (Fig. 14).

Based on the above temperature estimates, the crest of the anthophyllite–gedrite miscibility gap should be below 625° and above 570° and it is tentatively placed at 600±25°C, as shown in Figure 14. The solvus is asymmetrical, with the anthophyllite-rich limb being steeper than the gedrite-rich limb.

Conclusions

Orthoamphiboles are found in a wide variety of geologic environments. Careful delineation of the solvus in T–X space will enable metamorphic temperatures to be estimated in samples where two orthoamphiboles coexist. Additional data on natural samples coupled with experimental determination will serve to refine the T–X solvus presented in Figure 14. Exsolution features in sub-solvus and super-solvus orthoamphiboles may also reveal information on cooling rates (Ross *et al.*, 1969; Robinson *et al.*, 1971b).

Acknowledgments

Most of the analytical work for this study was conducted at the Geophysical Laboratory, Carnegie Institution of Washington, where the author was a Postdoctoral Fellow. Support from this Institution is gratefully acknowledged. Also acknowledged are many fruitful discussions with J. Ferry, J. Stout, L. Finger, E. Stoddard, and H. S. Yoder, Jr. The manuscript was improved considerably by constructive reviews by P. Robinson, M. Ross, and C. Klein. Special thanks go to D. Rumble, III, who contributed much time and energy both in the field and in the laboratory and who contributed several samples used in this study. Support of NSF grant EAR-79-11166 is also gratefully acknowledged.

References

Abraham, K. and W. Schreyer (1973) Petrology of a ferruginous hornfels from Rieckensgluck, Harz Mountains, Germany. *Contrib. Mineral. Petrol., 40,* 275–292.

Albee, A. L. and L. Ray (1970) Correction factors for electron probe microanalysis of silicates, oxides, carbonates, phosphates and sulfates. *Anal. Chem., 42,* 1408–1414.

Bence, A. E. and A. L. Albee (1968) Empirical correction factors for the electron microanalysis of silicates and oxides. *J. Geol., 76,* 382–403.

Bottinga, Y. and M. Javoy (1973) Comments on oxygen isotope geothermometry. *Earth Planet. Sci. Lett., 20,* 250–265.

Brady, J. B. (1974) Coexisting actinolite and hornblende from west-central New Hampshire. *Am. Mineral., 59,* 529–535.

Deer, W. A., R. A. Howie and J. Zussman (1963) *Rock-Forming Minerals, v. 2: Chain Silicates.* Longmans, London.

Downs, W. F. and P. Deines (1978) Experimental calibration of the quartz–magnetite oxygen isotope geothermometer (abstr.). *Geol. Soc. Am. Abstracts with Programs, 10,* 392.

Ferry, J. M. and F. S. Spear (1978) Experimental calibration of the partitioning of Fe and Mg between biotite and garnet. *Contrib. Mineral. Petrol., 66,* 113–117.

Finger, L. W. (1970) Refinement of the crystal structure of an anthophyllite. *Carnegie Inst. Wash. Year Book, 68,* 283–288.

Gable, D. J. and P. K. Sims (1970) Geology and regional metamorphism of some high grade cordierite gneisses, Front Range, Colorado. *Geol. Soc. Am. Spec. Pap. 128.*

Gittos, M. F., G. W. Lorimer and P. E. Champness (1976) The phase distributions in some exsolved amphiboles. In H.-R. Wenk, Ed., *Electron Microscopy in Mineralogy,* p. 238–247. Springer-Verlag, Berlin.

Hadley, J. B. (1942) Stratigraphy, structure and petrology of the Mt. Cube area, New Hampshire. *Geol. Soc. Am. Bull., 53,* 113–176.

Holdaway, M. J. (1971) Stability of andalusite and the aluminum silicate phase diagram. *Am. J. Sci., 271,* 97–131.

——— and Sang Man Lee (1977) Fe–Mg cordierite stability in high-grade pelitic rocks based on experimental, theoretical and natural observations. *Contrib. Mineral. Petrol., 63,* 175–198.

James, R. S., R. A. F. Grieve and L. Pauk (1978) The petrology of cordierite–anthophyllite gneisses and associated mafic and pelitic gneisses at Manitouwadge, Ontario. *Am. J. Sci., 278,* 41–63.

Kamineni, D. C. (1975) Chemical mineralogy of some cordierite-bearing rocks near Yellowknife, Northwest Territories, Canada. *Contrib. Mineral. Petrol., 53,* 293–310.

Klein, C., Jr. (1969) Two-amphibole assemblages in the system actinolite–hornblende–glaucophane. *Am. Mineral., 54,* 212–237.

Lal, R. K. and W. W. Moorhouse (1969) Cordierite–gedrite rocks and associated gneisses of Fishtail Lake, Harcourt Township, Ontario. *Can. J. Earth Sci., 6,* 145–165.

Leake, B. E. (1978) Nomenclature of amphiboles. *Can. Mineral., 16,* 501–520.

Papike, J. J. and M. Ross (1970) Gedrites: crystal structures and intercrystalline cation distributions. *Am. Mineral., 55,* 1945–1972.

Rabbitt, J. C. (1948) A new study of the anthophyllite series. *Am. Mineral., 33,* 263–323.

Robinson, P. and H. W. Jaffe (1969) Chemographic exploration of amphibole assemblages from central Massachusetts and southwestern New Hampshire. *Mineral. Soc. Am., Spec. Pap. 2,* 251–274.

———, ———, C. Klein, Jr. and M. Ross (1969) Equilibrium coexistence of three amphiboles. *Contrib. Mineral. Petrol., 22,* 248–258.

———, M. Ross and H. Jaffe (1970) The composition field of anthophyllite and the anthophyllite miscibility gap (abstr). *Am. Mineral., 55,* 307–309.

———, ——— and ——— (1971a) Composition of the anthophyllite–gedrite series, comparisons of gedrite and hornblende, and the anthophyllite–gedrite solvus. *Am. Mineral., 56,* 1005–1041.

———, H. Jaffe, M. Ross and C. Klein, Jr. (1971b) Orientation of exsolution lamellae in clinopyroxenes and clinoamphiboles: consideration of optimal phase boundaries. *Am. Mineral., 56,* 909–939.

Ross, M., J. J. Papike and K. Wier Shaw (1969) Exsolution textures in amphiboles as indicators of sub-solidus thermal histories. *Mineral. Soc. Am., Spec. Pap. 2,* 275–299.

Rumble, D. (1969) *Stratigraphic, Structural and Petrologic Studies in the Mt. Cube area, New Hampshire.* Ph.D. Dissertation, Harvard University, Cambridge, Massachusetts.

Seki, Y. and M. Yamasaki (1957) Aluminian ferroanthophyllite from the Kitakami Mountainland, northeastern Japan. *Am. Mineral., 42,* 506–520.

Spear, F. S. (1977) Phase equilibria of amphibolites from the Post Pond Volcanics, Vermont. *Carnegie Inst. Wash. Year Book, 76,* 613–619.

——— (1978) Petrogenetic grid for amphibolites from the Post Pond and Ammonoosuc Volcanics. *Carnegie Inst. Wash. Year Book, 77,* 805–808.

——— (1980) NaSi⇄CaAl exchange equilibrium between plagioclase and amphibole: an empirical model. *Contrib. Mineral. Petrol., 72,* 33–41.

Stoddard, E. F. (1979) Phase petrology of cordierite–amphibole rocks, Old Woman–Piute Range, Southeastern California (abstr.). *Geol. Soc. Am. Abstracts with Programs, Cordilleran Section, 11,* 130.

Stout, J. H. (1969) An electron microprobe study of coexisting orthorhombic amphiboles (abstr.). *Trans. Am. Geophys. Union, 50,* 359.

——— (1970) Three-amphibole assemblages and their bearing on the anthophyllite–gedrite miscibility gap (abstr.). *Am. Mineral., 55,* 312–313.

——— (1971) Four coexisting amphiboles from Telemark, Norway. *Am. Mineral., 56,* 212–224.

——— (1972) Phase petrology and mineral chemistry of coexisting amphiboles from Telemark, Norway. *J. Petrol., 13,* 99–145.

Thompson, A. B. (1976) Mineral reactions in pelitic rocks: II. Calculation of some *P–T–X* (Fe–Mg) phase relations. *Am. J. Sci., 276,* 425–454.

Thompson, J. B., Jr., P. Robinson, T. N. Clifford and N. J. Trask (1968) Nappes and gneiss domes in west-central New England. In E-an Zen *et al.,* Eds., *Studies of Appalachian Geology,* p. 203–218. Wiley, New York.

Tracy, R. J., P. Robinson and A. B. Thompson (1976) Garnet composition and zoning in the determination of temperature and pressure of metamorphism, central Massachusetts. *Am. Mineral., 61,* 762–775.

Manuscript received, November 9, 1979;
accepted for publication, May 7, 1980.